3D Left-Ventricular Deformation Analysis from 3D CSPAMM with 3D SinMod

Hui Wang[1], Christian T. Stoeck[2], Sebastian Kozerke[2], and Amir A. Amini[1]

[1]University of Louisville, Louisville, KY, United States, [2]Institute for Biomedical Engineering, ETH, Zurich, Switzerland

Introduction

Tagged MRI of the heart provides a useful way for estimating cardiac motion fields and cardiac mechanical function [1-3]. A number of approaches have been proposed for analysis of cardiac motion from tagged MRI [4]. Among these, frequency-based methods have seen wider applicability for analysis of displacement and mechanical properties of the myocardium [5, 6]. Most of the current techniques are applicable to 2D+t tagged MR image sequences. In this abstract, we propose a novel 3D sine wave modeling (3D SinMod) approach for automatic analysis of 3D cardiac deformations from 3D complementary spatial modulation of magnetization (CSPAMM) MRI [7]. The entire framework from data acquisition to data analysis is in 3D, permitting quantification of both the in-plane and through-plane components of motion.

Methods

MR tagging gives rise to spectral peaks in k-space, each spectral peak containing information about motion in a particular direction. In 3D SinMod, the intensity distribution around each voxel in 3D volume is modeled as a cosine wave front with local frequency and amplitude. $V_1(x, y, z) = A_1 \cos(\omega_x(x + u/2) + \varphi) + n_1(x, y, z), V_2(x, y, z) = A_2 \cos(\omega_x(x - u/2) + \varphi) + n_2(x, y, z)$ where ω_x and φ are the spatial frequency and phase of the wave respectively, and A_1 and A_2 are wave magnitudes for the first 3D volume V_1 and the second 3D volume V_2, while n_1 and n_2 are additive noise. u corresponds to the displacement between these two volumes at position (x, y, z) along the x direction. Repeating the same algorithm on image volumes in the other directions yields 3D displacement. The principle behind SinMod tracking is that both phase and frequency for each voxel are determined directly from the frequency analysis and the displacement is calculated from the quotient of phase difference and local frequency. After obtaining the Fourier transform of the input volumes $V_1(x, y, z)$ and $V_2(x, y, z)$ (temporal frames at time point n and time point $n + 1$), identical 3D band-pass filters are applied to both volumes to isolate corresponding spectral peaks in order to produce a pair of complex volumes in the Fourier domain. Let us refer to the two complex volumes in Fourier domain following band-pass filtering as $\gamma_{bf1}(\omega_x, \omega_y, \omega_z)$ and $\gamma_{bf2}(\omega_x, \omega_y, \omega_z)$. Applying a low frequency band-pass filter and a high frequency one to both γ_{bf1} and γ_{bf2} followed by an inverse Fourier transform leads to four complex volumes $V_{bfLf1}(x, y, z)$, $V_{bfHf1}(x, y, z)$, $V_{bfLf2}(x, y, z)$, and $V_{bfHf2}(x, y, z)$. The LPF and HPF are applied to γ_{bf1} and γ_{bf2} in order to determine the local spatial frequency by power spectra. Then the displacement is the local quotient of phase difference and local frequency at that position. The power spectra and cross power spectrum are given by: $P_{Lf}(x, y, z) = |V_{bfLf1}|^2 + |V_{bfLf2}|^2$, $P_{Hf}(x, y, z) = |V_{bfHf1}|^2 + |V_{bfHf2}|^2$, $P_{cc}(x, y, z) = V_{bfHf1}\overline{V_{bfLf2}} + V_{bfHf1}\overline{V_{bfHf2}}$ where $\overline{V}$ is the complex conjugate of V. The local frequency ω_x and local displacement u can then be estimated from: $\omega_x(x, y, z) = \omega_c\sqrt{P_{Hf}/P_{Lf}}$, $u(x, y, z) = \arg(P_{cc})/\omega_x$.

Results

An accelerated 3D CSPAMM tagging technique [7] was used to modulate the magnetization of myocardial tissue in three orthogonal tagline directions and acquire data in the entire left ventricle (LV) within three breath-holds. Five in-vivo 3D+t CSPAMM data sets from healthy volunteers were used to validate the proposed 3D SinMod algorithm. For each dataset, 20-24 time frames were acquired, with each volume consisting of 14 slices. Left ventricular endocardial and epicardial contours were traced manually at all phases for each 3D data set. The 3D motion fields at end-systole are shown in Figure 1(a) for apex, apical, mid-cavity, and basal slices. Figure 1 (b), (c), (d), and (e) are the projected 2D end-systolic motion fields on the corresponding slices. All tag lines on 11 slices (from apex to base) and over 11 systolic phases in each data set were manually delineated. Subsequently, the manually delineated tag lines from each time were warped to time t+1 with 3D SinMod and the location of the warped tag lines were compared to locations of manually delineated tag lines and an average error for each phase was computed. Figure 2 displays the average error as function of time for each of the 5 data sets. The average CPU time for calculating 3D motion fields between a pair of 3D volumes for each of the data sets was 17.37 seconds on a conventional PC (Intel Core i5 2.6 GHz CPU/4 GB main memory).
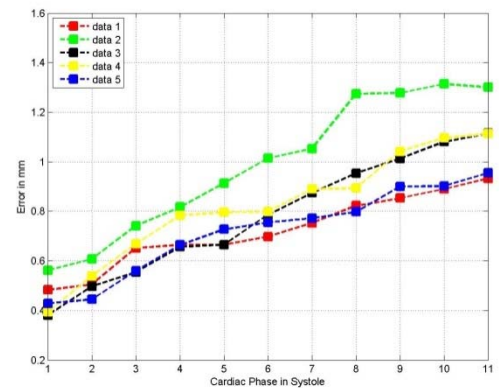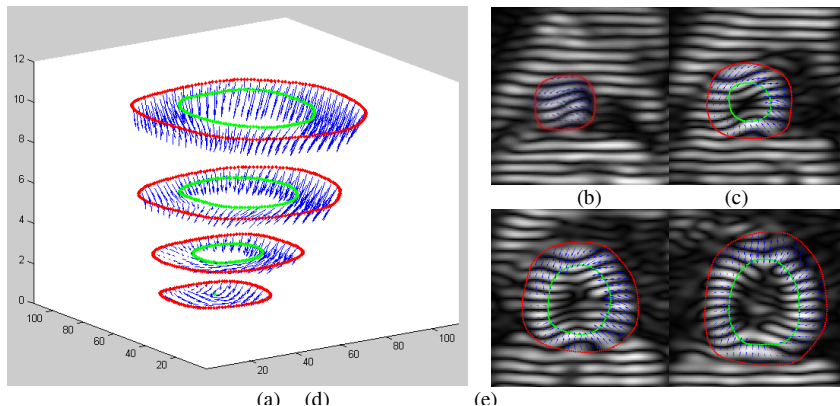

Figure 1. (a) The calculated 3D motion fields on apex, apical, mid-cavity, and basal slices. The projected 2D end-systole motion fields are displayed in (b)-(e).

Figure 2. 3D SinMod's average error as a function of time for determining tag line displacements during systole for 5 in-vivo data sets.

Discussion

A novel 3D SinMod algorithm for analysis of 3D myocardial deformations using 3D CSPAMM acquisition has been proposed. The proposed framework permits accurate and automatic determination of both in-plane and through-plane components of motion of the LV myocardium. The deformation fields clearly demonstrate longitudinal shortening during systole. The contraction of the LV base towards the apex as well as the torsional motion between basal and apical slices is clearly observable from the displacements.

References

1. Zerhouni E. A. etc., *Radiology*, 169(1): 59-63; 1988. 2. Axel L. and Dougherty L., *Radiology*, 171(3): 841-845; 1989. 3. Fischer S. E. et al., *Magn. Reson. Med.*, 31(2):191-200; 1993. 4. Wang H. and Amini A., *IEEE Trans. on Med. Imag.*, 31(2):487-503; 2012. 5. Osman N. F. et al., *Magn. Reson. Med.*, 42(6):1048-1060; 1999. 6. Arts T. et al., *IEEE Trans. on Med. Imag.*, 29(5):1114-1123; 2010. 7. Rutz A. et al. *Magn. Reson. Med.*, 59(4):755-763; 2008